



PIV MEASUREMENTS IN TWIN SYNTHETIC JETS

C. S. GRECO[°], A. IANIRO, M. IMBRIALE, T. ASTARITA, G. CARDONE

Department of Aerospace Engineering, University of Naples Federico II, 80125 via Claudio 21, Napoli, Italy

[°] Corresponding author: Tel.: +39 329 9513504 - +39 081 768 3389; Email: carlo.greco@studenti.unina.it

KEYWORDS:

Main subjects: flow visualization and flow field measurements

Fluid: air

Visualization method: PIV phase averaged measurements

Other keywords: Synthetic jets and turbulence

ABSTRACT: In this work a double synthetic jet configuration is experimentally investigated. The oscillating membrane is a subwoofer membrane that splits the cavity in two sub-cavities with the same resonance frequency. Each cavity is connected to the quiescent ambient by a cylindrical nozzle thus two jets in phase opposition are obtained. The influence of jet interactions has been evaluated, while the jets pulsating frequency is kept equal to the sub-cavities resonance frequency. Moreover the flow is characterized with PIV measurement; in particular the stroke length L_0 and consequently the Reynolds number are evaluated. Phase averaged measurements are presented: the classical behaviour of the single synthetic jet is confirmed while the interaction of the two synthetic jets seems to have a positive effect on the jets development.

INTRODUCTION. Synthetic jets are particular jets with zero-net-mass flux. Typically a synthetic jet is generated due to a periodic membrane movement in a cavity that causes the formation of a train of vortices at a nozzle exit, which is connected with the cavity. In recent studies, a wide variety of vibrating actuators have been employed as membrane, including piezoelectric diaphragm [1,2,3], pistons electromagnetically moved [4,5] and cavities acoustically driven [6,7]. The membrane is usually enclosed in a cavity and its periodic movement produces a periodic pressure variation. As the membrane oscillates, fluid is periodically entrained into the cavity and then expelled through the nozzle completing the cycle. During the injection portion of the cycle the flow field may be considered as the induced by a sink, which coincides with the nozzle exit, while during the expulsion portion of the cycle, a vortex ring can form near the nozzle and, under certain operating conditions [8], convects away from the orifice to form a time averaged-jet in a limited zone near its axis [9,10]. The first to develop a theory on this topic was Helmholtz [11] that gave the name to the Helmholtz resonators. The approximate Helmholtz theory is based upon the hypothesis that the orifice (whose outline is circular or elliptic) is small and consequently that the wavelength of the aerial vibration is great compared to the orifice characteristic length. Lord Rayleigh [12] gave a more simplified and generalised treatment and explained mathematically the theory on which Helmholtz resonators are based [11]. The results, obtained by Lord Rayleigh, differ from that given by Helmholtz since the aperture in the cavity is supposed to be surrounded by an infinite flange whose effect is to promote the propagation of energy away from the resonator. Subsequently Lightill [10] investigated how turbulent jets could be generated by a sound and suggested two methods for generating fluid streams. The first is based on the transmission of pressure waves through a compressible medium while the second is related to viscous effects at a boundary. While the studies on acoustic streaming date very old [11,12], only in the last decades the knowledge about this topic received a great improvement. Smith and Glezer [9] studied the formation and evolution of synthetic jets comparing them to conventional 2-D jets. According to them the streamwise decrease of the synthetic jet mean centerline velocity is higher and the streamwise increase of its width and volume flow rate is lower. Cater and Soria [13] investigated experimentally a round zero-net-mass-flux jet observing that it has a cross-stream velocity distribution similar to that of a conventional continuous jet but with a larger spreading rate and decay constant. Recently synthetic jets have been increasingly used for flow control so both experimental and numerical studies are focused on it. Smith and Glezer [14] studied how a synthetic jet can be used to create a jet vectoring. They investigated experimentally the interaction between a conventional rectangular air jet and a co-flowing synthetic jet, using particle image velocimetry, observing that the continuous jet fluid was deflected toward the synthetic jet and the interaction between the jets leads to the formation of a closed recirculating flow domain. Smith and Glezer [15] also studied the interaction of two

adjacent synthetic jets that are driven by phase-shifted signals using particle image velocimetry. These two synthetic jets create a different flow field related to the existing phase angle between the actuation waveforms of the adjacent jets. The obtained results show that the phase variation leads to controlled vectoring of the combined jets toward the nozzle exit of the jet that is leading in phase and that the degree of vectoring increases with phase angle until the merged jets flow along the surface of the exit plane. After a certain phase angle the degree of vectoring starts decreasing.

Synthetic jets were also successfully studied for their potential to be applied in impingement heat transfer applications. Valiorgue et al. [16], Chaudhari et al. [17] and Arik [18] worked on synthetic jets used to cool a heated surface and showed that synthetic jets allow to obtain huge values of the local heat transfer coefficient. Lately Persoons et al. [19] found also a general correlation for the stagnation point heat transfer performance for a wide parameter range such as Reynolds number, nozzle-to-surface distance and stroke length. Synthetic jets are usually investigated in the classical single configuration but recent works are focusing on different configurations such as double [20] and asymmetric configurations [21]. Lasance et al. [22] carried out experiments using a double jet configuration in order to establish its heat transfer performance for a range of frequencies, nozzle, in form of a pipe, lengths and diameters and by comparison with a standard fan and synthetic jets show promising performances for electronic cooling applications [23]. Such results are obtained for a twin synthetic jets in which a standard loudspeaker splits cavity in two sub-cavities generating two opposite-phase synthetic jets which provide a significant noisy reduction. For this reason the interest in studying twin synthetic air jets formation and evolution can be justified although Smith and Glezer [15] suggested that when the phase angle is close to 180 deg the instantaneous flow is predominantly characterized by alternating flows out of and into adjacent cavities with relatively weak time-averaged flow without any interesting features. In this work a double cavity for twin synthetic jet is designed, acoustically characterized and experimentally studied. The study is performed by using PIV technique and in the following both averaged and phase averaged flow field are described.

SYNTHETIC JET APPARATUS. Fig. 1 shows a typical sketch of a dipole cooler showing the two pipes attached to both sides of a single loudspeaker with a diameter of 270 mm. The loudspeaker splits the cavity in two sub-cavities with the same Helmholtz resonance frequency therefore the jets are in opposite phase and this allows to decrease synthetic jet noise. The two sub-cavities have the same resonance frequency because the volumes V_1 and V_2 (size about $\sim 2 \text{ dm}^3$) at both sides are equal, which is obtained realizing a conical frustum inside the two sub-cavities. The jet exit pipes have an inner diameter of 21 mm and a length of 210 mm, thus the two sub-cavities should have, according to (1), a Helmholtz resonance frequency [11] of about 46 Hz:

$$f_H = \frac{c}{2\pi} \cdot \sqrt{\frac{\pi D^2/4}{V \cdot L}} \quad (1)$$

where f_H is Helmholtz resonance frequency, c is air speed of sound, $\pi D^2/4$ is tube cross section area, V is sub-cavity volume and L is tube length.

Actually they show a resonance frequency of about 10.6 Hz as shown in Fig. 2 from the plot of the stagnation pressure

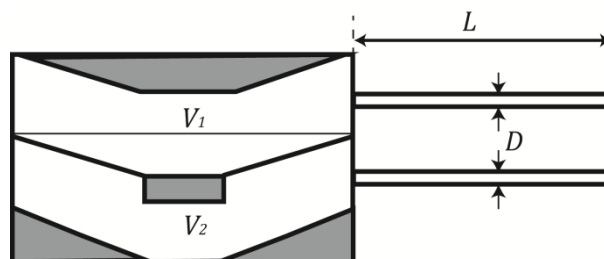


Figure 1 Sketch of the synthetic jet apparatus

PIV MEASUREMENTS IN TWIN SYNTHETIC JETS

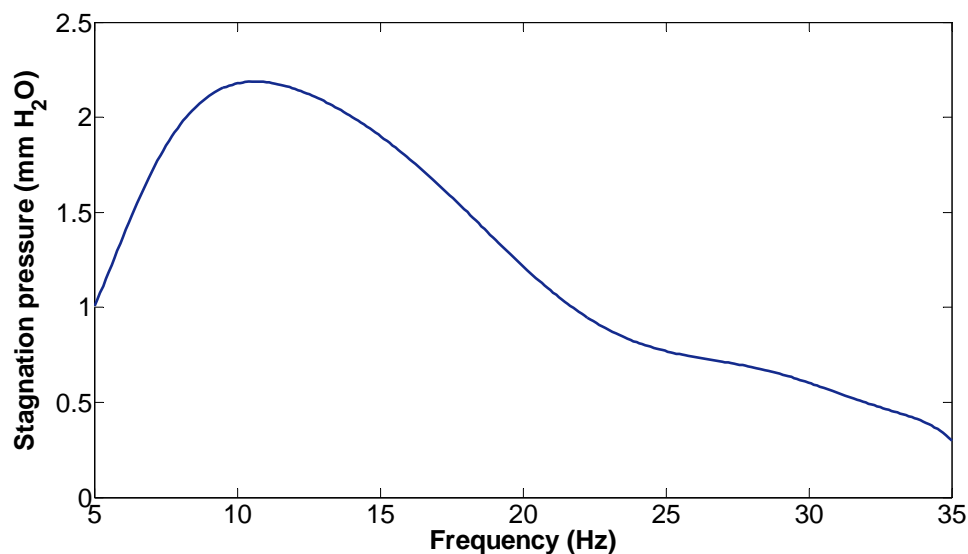


Figure 2 Stagnation pressure versus frequency

on the jet axis versus frequency. The discrepancy should be ascribed to the sub-cavities geometry that is highly irregular and three-dimensional and to the nozzle exits that are not located opposite to the oscillating membrane. According to Chanaud [24, 25] the value of the Helmholtz resonance frequency is not simply related to the cavity volume but is related also to its shape, i.e. depth, width and breadth. Furthermore the position of the nozzle exit can influence that frequency and also the choice of the surface on which the nozzle is located can cause a change of the Helmholtz resonance frequency. In particular Chanaud [24] shows that the Helmholtz resonance frequency decreases proportionally to the increase of distance between the nozzle and the centre of the face of the cavity opposite to the membrane up to a maximum of 40%. Hence for our sub-cavities, where the orifice is located on a surface that is not opposite to the oscillating membrane, the Helmholtz resonance frequency should decrease at least of 40% due to the complete loss of symmetry in the cavity. Alster suggests [26] that also the cavity geometry can introduce a displacement from the theoretical Helmholtz resonance frequency. As previously said, each of the two sub-cavities has a geometry similar to a conical frustum: this, according to Alster, makes the resonance frequency decrease of about 50% with respect to the theoretical Helmholtz resonance frequency. The difference between the measured and theoretical Helmholtz resonance frequency of our dipole cooler is in agreement to what reported by Lasance et al [22]: their dipole cooler shows an actual resonance frequency that is about one fifth of the theoretical Helmholtz resonance frequency.

FLOW FIELD CHARACTERIZATION BY PIV TECHNIQUE. In order to obtain quantitative information about the flow field, jet development and interactions and to measure characteristic quantities such as Reynolds number and stroke length, Particle Image Velocimetry measurements are performed. The synthetic jet is controlled by the sound card of a personal computer. The input signal, generated by the PC, is a sinusoidal signal with a frequency f_i of 10 Hz that, before reaching the loudspeaker, is intensified by an amplifier in order to obtain an output voltage of about 7.5 V and an output current of about 1.9 A. Three jet-axes-distances are used for the flow field measurements and the experimental setup is sketched in Fig. 3. The light sheet, which is generated by a double cavity Nd-YAG laser, has a thickness of about 0.5 mm, a pulse duration of about 2 ns, a wavelength of 532 nm and an energy per pulse of about 150 mJ. To display, acquire and record 2D images with a spatial resolution of 6 pixels/mm, a video camera PCO sensicam (with a CCD sensor of 1024x1280 pixels, 4096 grey levels, and a 50 mm Nikon objective, $f/\# = 8$) is used and oil droplets of about 1 μm in diameter are used to seed the flow. In order to obtain reliable turbulence statistics 6000 double frame images are taken for each test. The imaging system is synchronized with the synthetic jet in order to perform phase-averaged measurements. The same computer that provides the signal to the loudspeaker generates also a trigger signal for the PIV system.

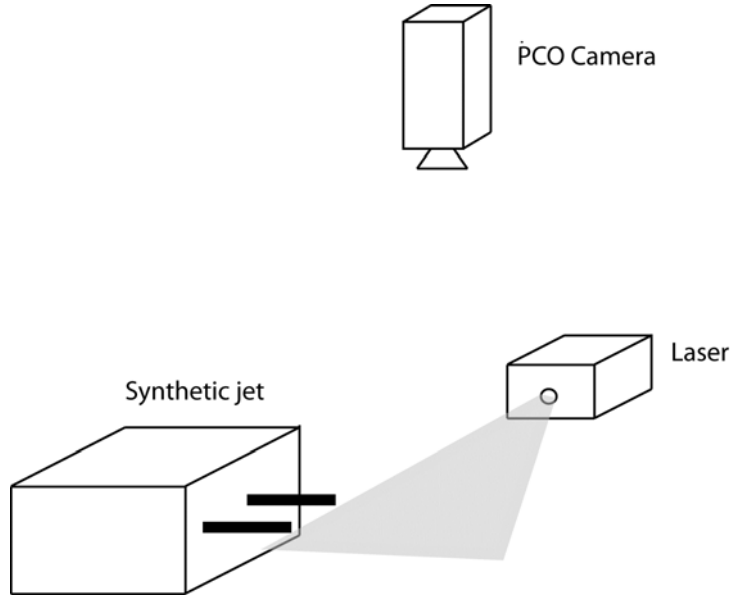


Figure 3 Experimental setup

The acquisition is performed at a frequency lower than 1 Hz, sampling the phenomenon every $n = 10$ periods with a phase shift of $360^\circ / NDiv$ (where $NDiv=30$ is the number of the phases which are sampled) thus the trigger signal is given at a frequency f_2 equal to:

$$f_2 = \frac{f_1}{\frac{1}{NDiv} + n} \quad (2)$$

In this way synthetic jet is sampled at each 12 degrees of phase variation and 200 images are acquired for each phase. The flow field has been obtained processing images captured by CCD camera according to Astarita and Cardone [27] and Astarita [28, 29] with a final interrogation window size of 24x24 pixels and an overlap of 6 pixels thus producing a vector pitch of 1mm. Phase averaged flow field are used to evaluate stroke length L_0 as:

$$L_0 = \int_0^{T/2} U_A(t) dt \quad (3)$$

where T is the actuation period and $U_A(t)$ is the exit velocity on the jet axis. Subsequently the reference velocity U_0 is calculated as:

$$U_0 = \frac{L_0}{T} \quad (4)$$

Following [9] the Reynolds number can be obtained as:

$$Re = \rho \cdot U_0 \cdot D / \mu \quad (5)$$

where ρ is the air density and μ is the air dynamic viscosity.

AVERAGED FLOW FIELD. In Fig. 4 are presented the averaged flow fields obtained for a single jet and for double jet configurations with jet-axes-distance l of 1, 3 and 5 diameters respectively: in particular Fig. 4 shows a contour of axial velocity with vector arrows on the left and a contour of the Reynolds stresses $\overline{U'U'}/U_0^2$ on the right. Each experimental test is carried out providing a power of about 14 W with an accuracy of about 3%. Reynolds numbers obtained for single jet and double jet configurations are 4300, 5600, 5500 and 5400 respectively and the stroke lengths are 0.3 m, 0.39 m, 0.38 m and 0.37 m respectively. The single jet configuration, obtained deflecting one of the two

PIV MEASUREMENTS IN TWIN SYNTHETIC JETS

synthetic jets by using a bended tube at the exit of the orifice, shows a Reynolds number lower than that relative to the double jet configurations. This is related to the presence of the bended tube at the exit which causes a significant change of the Helmholtz resonance frequency of one sub-cavity that results in only the tested sub-cavity working in resonance condition. The Reynolds number increases when jet-axes-distance decreases.

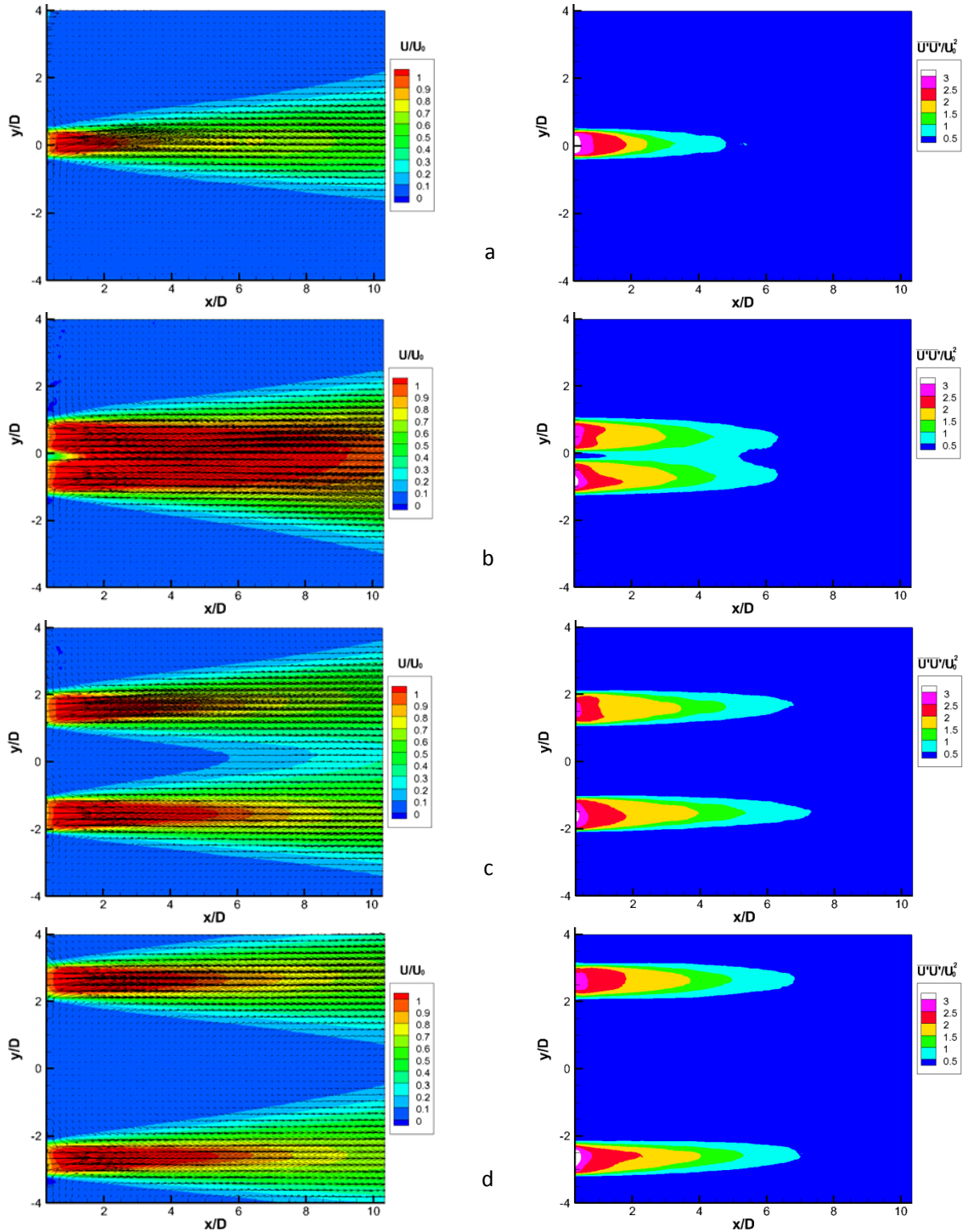


Figure 4 Averaged flow field with vector arrows and contour on the left and Reynolds stresses on the right for a) single jet configuration, b) double jet configuration with $l = 1 D$, c) with $l = 3 D$ and d) with $l = 5 D$

This effect can be ascribed to the fact that, as shown in phase-averaged measurements, the suction cycle of one jet influences the expulsion cycle of the other jet, making the velocity of the latter increase. In double jet configuration, $l = 1 D$, there is an abrupt interaction between the two averaged jets which leads to obtain an almost merged jet on the symmetry axis of the field close to the exit-tube-plane. It has to be evidenced that the Reynolds stresses merge later with respect to the mean velocity. Moreover in double jet configuration with a jet-axes-distance of 3 diameters the two averaged jets get merged at a distance, from the exit-tube-plane, of about 8 diameters. Regarding to Reynolds stresses one can point out that synthetic jets show maximum values of such stresses on the axis of the jet and near the exit-tube-plane differently from a continuous jet in which maximum values of such stresses are located on the boundary of the jet while minimum values are near the exit-tube-plane [30] and turbulent fluctuations mostly develop from the shear layer.

PHASE-AVERAGED FLOW FIELD. In Figs. 5, 6, 7 and 8 the evolution of the single and double synthetic jet (in all the configurations) are shown. Only 15 phases are presented corresponding to a 24 degrees phase variation. For the single jet configuration it is possible to highlight that the evolution of the synthetic jet agrees to previous studies [9]. Indeed, during the expulsion cycle, one can notice the presence of the ring vortex, which develops from the nozzle exit, and that the maximum velocity is positioned in vortex centre because the entrainment, caused by the ring vortex, is stronger in that zone. In addition to that, during the suction cycle the flow field is characterized by the presence of a saddle point which has not always the same x/D station and reaches a maximum distance, from the tube exit, of about 2 diameters. During the suction cycle the flow field is divided, by the presence of the saddle point, in two sub-flow-fields which show opposite sign of the axial-velocity. The 180° phase shift existing between the two jets is clearly visible in Figs. 6, 7 and 8. Indeed when one sub-cavity generates its synthetic jet the other one starts the suction cycle. In this double jet configuration each jet is deflected towards the centre of the flow field because of the influence of the suction cycle of the other jet. This deflection increases with decreasing jet-axes-distance because such decrease leads to intensifying the influence of the suction zone on the ejection zone. Obviously also in double jet configuration each jet shows, in the expulsion cycle, ring vortices surrounding it and the velocity maximum is also positioned in the centre of the vortex; a saddle point is observed during its suction cycle. In Fig. 6, $l = 5 D$, it is possible to see that while the first jet, the bottom one, is generating the second one is already characterized by higher velocities ($\varphi=0^\circ$). In the subsequent images one can notice, for the bottom jet, the creation of the ring vortex, at the tube exit, which causes an increase of velocity near it. The ring vortex is convected until the end of the field of view (from $\varphi=24^\circ$ to $\varphi=144^\circ$). During this period the other tube is characterized by the suction cycle. That influences the already formed jet slightly deflecting it towards the centre of the field (from $\varphi=96^\circ$ to $\varphi=144^\circ$). This phenomenon is more evident for $l = 3 D$ (Fig. 7 from $\varphi=72^\circ$ to $\varphi=144^\circ$) and even more for $l = 1 D$ (Fig. 8 from $\varphi=48^\circ$ to $\varphi=144^\circ$). Moreover in these last cases the ring vortex of the jet interacts suddenly with the zone after the saddle point of the other jet. After this interaction the ring vortex shows a slight inclination evidenced in Fig. 7 with the white lines ($\varphi=72^\circ$, $\varphi=96^\circ$ and $\varphi=120^\circ$) and this effect is more visible for $l = 1 D$ Fig. 8 ($\varphi=48^\circ$, $\varphi=72^\circ$, $\varphi=96^\circ$ and $\varphi=120^\circ$).

CONCLUSIONS. In this work twin air synthetic jets have been experimentally studied. The twin synthetic jets cavities have been designed in order to obtain a certain value of theoretical Helmholtz resonance frequency. The theoretical Helmholtz resonance frequency is different from the measured resonance frequency because of the peculiar shape of the cavities and configuration of the nozzle. The averaged and phase averaged flow field of a single and double jet configurations have been experimentally analysed in order to study the phenomenon unsteadiness by using a phase locked PIV measurements and sampling the synthetic jet at each 12 degrees of phase shift. Each test has been carried out providing the same power equal to 14 W and Reynolds number obtained for single and double jet configurations with a jet-axes-distance of 1, 3 and 5 diameters is 4300, 5600, 5500 and 5400 respectively. The single jet configuration shows the lowest Reynolds number because only one of the two sub-cavities works in resonance condition. The existing difference between the Reynolds numbers of the double jet configurations is due to the jet-axes-distance. Indeed when such distance becomes smaller, the suction cycle of one jet influences further the expulsion cycle of the other jet, making the axial velocity of the latter increase slightly. Phase averaged measurements for the single jet are in agreement with literature results while the interaction mechanisms between the twin synthetic jet are described.

PIV MEASUREMENTS IN TWIN SYNTHETIC JETS

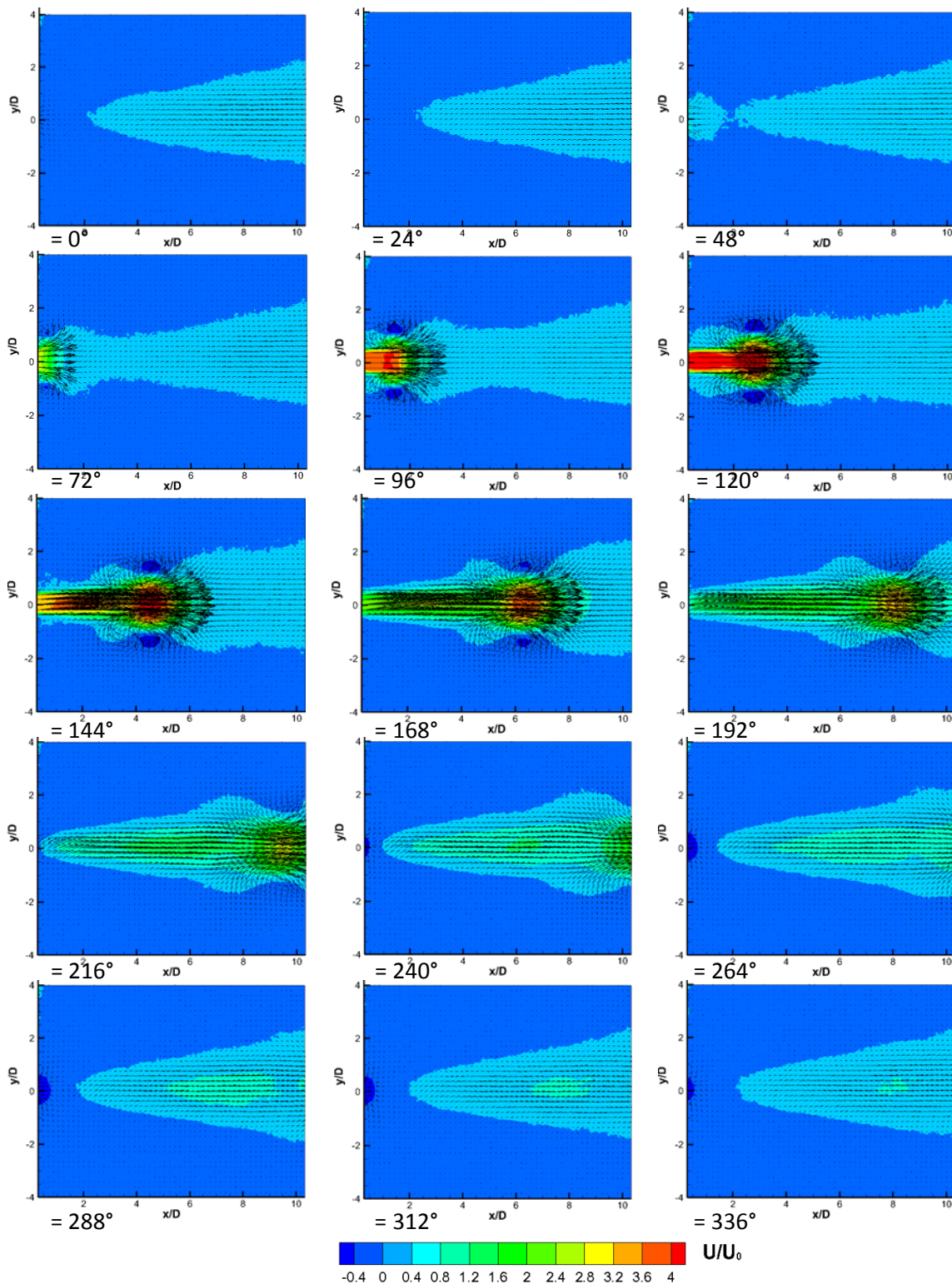


Figure 5 Phase averaged flow field for the single jet configuration

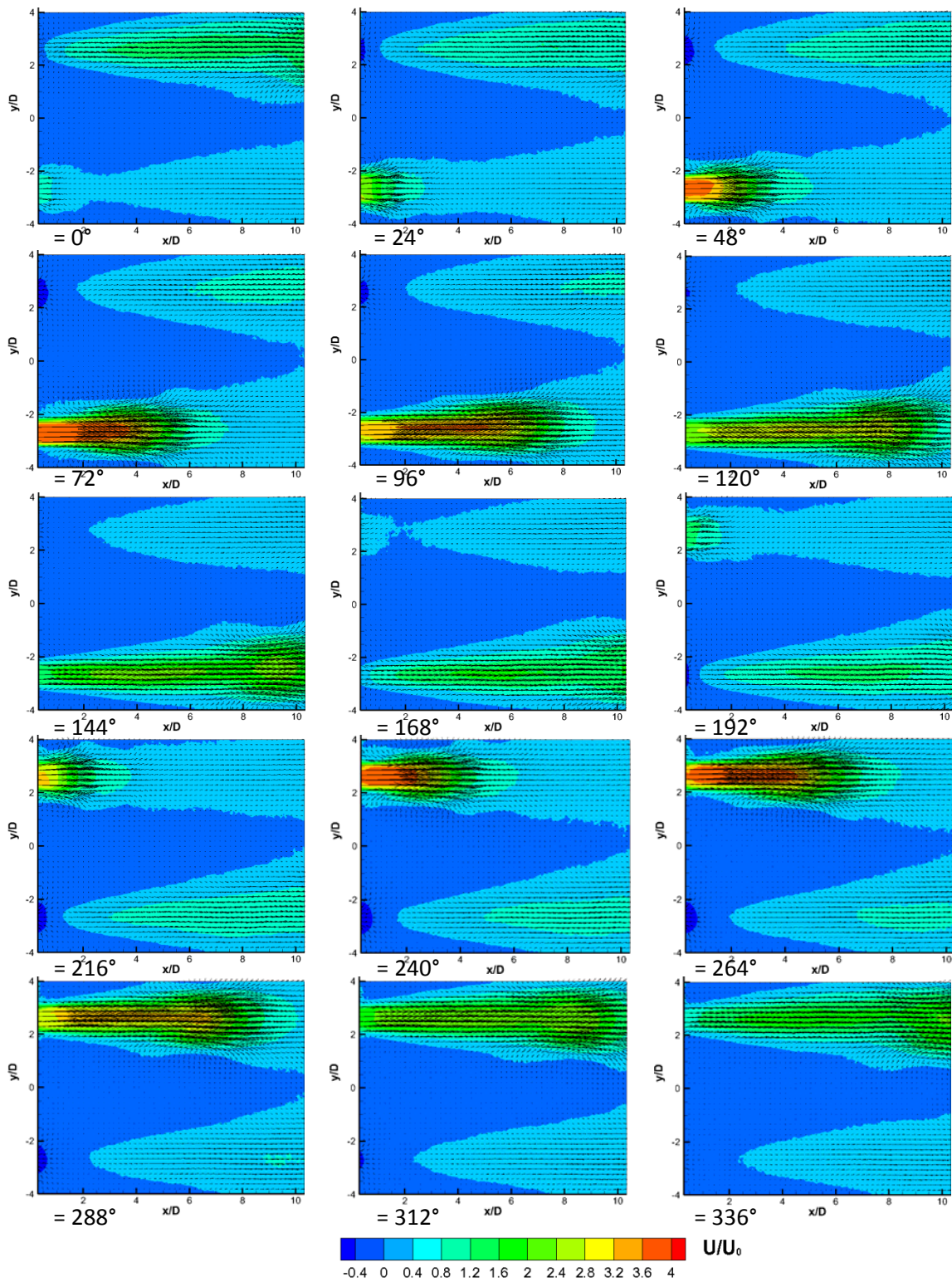


Figure 6 Phase averaged flow field for the double jet configuration with $l/D = 5$

PIV MEASUREMENTS IN TWIN SYNTHETIC JETS

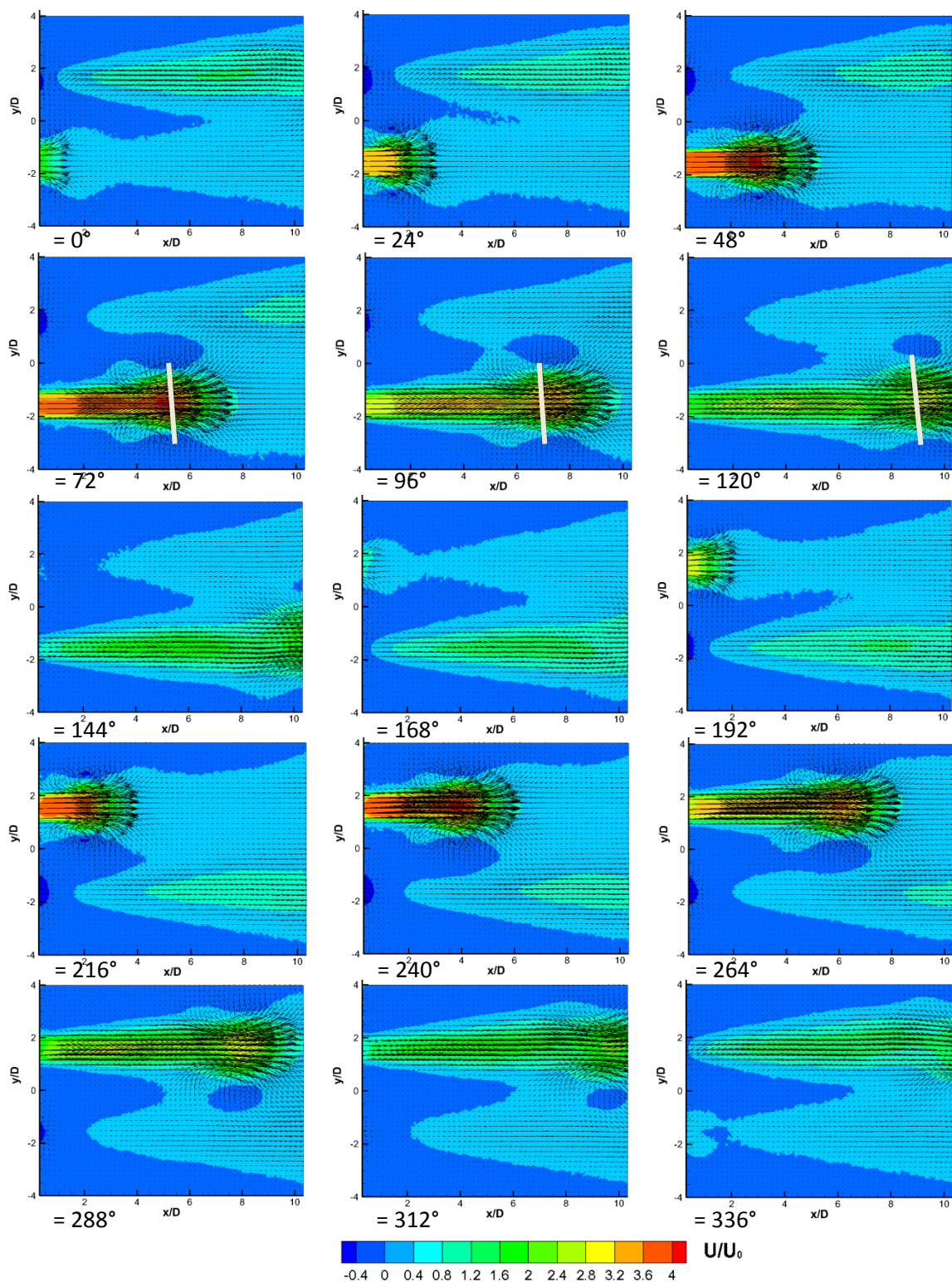


Figure 7 Phase averaged flow field for the double configuration with $l/D = 3$ with white lines identifying the plane on which the vortex ring lies

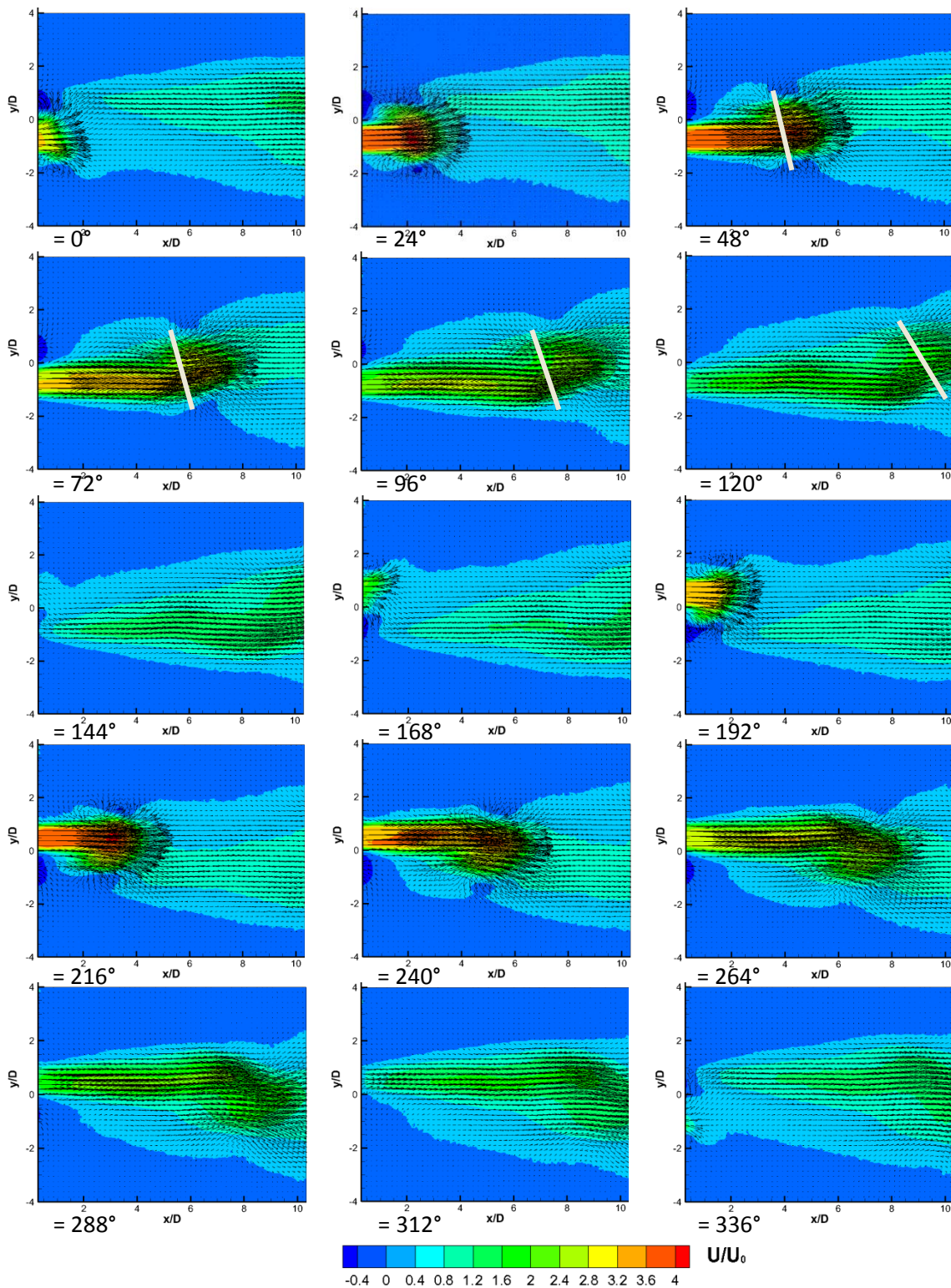


Figure 8 Phase averaged flow field for the double configuration with $l/D = 5$ with white lines identifying the plane on which the vortex ring lies

References

1. Mallison S.G. et al. *Some Characteristics of Synthetic Jets*. AIAA 28th Fluid Dyn. Conf 1999, p. 99
2. Crook A. et al. *The Development and Implementation of Synthetic Jets for Control of Separated Flow*. AIAA 17th Appl. Aerodyn. Conf. 1999, p. 99

PIV MEASUREMENTS IN TWIN SYNTHETIC JETS

3. Chen F.J. et al. *Development of Synthetic Jet Actuators for Active Flow Control at NASA Langley*. AIAA Fluid Meet. 2000, p. 2000
4. Rediniotis O.K. et al. *Synthetic Jets, Their Reduced Order Modeling and Applications to Flow Control*. AIAA 37th Aerosp. Sci. Meet. 2000, p. 2000
5. Crook A. and Wood N.J. *Measurements and Visualization of Synthetic Jets*. AIAA 39th Aerosp. Sci. Meet. 2001, p. 2001
6. Erk P.P. *Separation Control on a Post-Stall Airfoil Using Acoustically Generated Perturbations*. PhD thesis. Tech Univ. Berlin, Ger. 1997, p. 159.
7. McCormick D.C. *Boundary Layer Separation with Directed Synthetic Jets*. AIAA 38th Aerosp. Sci. Meet. 2000, p. 2000
8. Holman R. et al. *Formation Criterion for Synthetic Jets*. AIAA Journal 2005, **43** (10)
9. Smith B.L. and Glezer A. *The Formation and Evolution of Synthetic Jets*. Phys. Fluids 1998, **10** (9), p. 2281
10. Lighthill S.J. *Acoustic streaming*. J. Sound Vibration 1978, **61**, p. 391
11. Helmholtz H. *Theorie der Luftschwingungen in röhren mit offenen enden*. Crelle JI. Math. 1860 **57**, p. 1
12. Lord Rayleigh J.W.S. *The Theory of the Helmholtz Resonator*. Proc. R. Soc. Lond. 1916, **92**, p. 265
13. Cater J.E. and Soria J. *The evolution of round zero-net-mass-flux jets*. J. Fluid Mech. 2002, **472**, p. 167
14. Smith B.L. and Glezer A. *Jet vectoring using synthetic jets*. J. Fluid Mech. 2002, **458**, p. 1
15. Smith B.L. and Glezer A. *Vectoring of Adjacent Synthetic Jets*. AIAA Journal. 2005, **43** (10)
16. Valiorgue P. et al. *Heat Transfer Mechanisms in an Impinging Synthetic Jet for small Jet-to-Surface Spacing*. Experimental Thermal and Fluid Science 2009, **33**, p. 597.
17. Chaudhari M. et al. *Heat Transfer Characteristics of Synthetic Jet Impingement Cooling*. International Journal of Heat and Mass Transfer 2010, **53**, p. 1057
18. Arik M. *Local Heat Transfer Coefficients of High-Frequency Synthetic Jet during Impingement Cooling over Flat Surfaces*. Heat Transfer Engineering 2008, **29**, p. 763
19. Persoons T. et al. *A general correlation for the stagnation point Nusselt number of an axisymmetric impinging synthetic jet*. International Journal of Heat and Mass Transfer 2011, **54**, p. 3900
20. Lasance C.J.M. and Aarts R.M. *Synthetic Jet Cooling Part I: Overview of Heat Transfer and Acoustic*. 24th Annual IEEE Semiconductor Thermal Measurement and Management Symposium 2008, p. 20
21. Lasance C.J.M. et al. *Synthetic Jet Cooling Using Asymmetric Acoustic Dipoles*. 25th Annual IEEE Semiconductor Thermal Measurement and Management Symposium 2009, p. 254
22. Lasance C.J.M. et al. *Synthetic jet cooling part II: experimental results of an acoustic dipole cooler*. 24th Annual IEEE Semiconductor Thermal Measurement and Management Symposium 2008, p. 26
23. Mahalingam R. et al. *Synthetic Jets for forced air cooling of electronics*. Electronics Cooling 2007, **13** (2).
24. Chanaud R.C. *Effects of Geometry on the Resonance Frequency of Helmholtz Resonators*. Journal of Sound and Vibration 1994, **178** (3), p. 337
25. Chanaud R.C. *Effects of Geometry on the Resonance Frequency of Helmholtz Resonators, part II*. Journal of Sound and Vibration 1997, **204**(5), p. 829
26. Alster M. *Improved Calculation of Resonant Frequencies of Helmholtz Resonators*. Journal of Sound and Vibration 1972, **24**(1), p. 63
27. Astarita T. and Cardone G. *Analysis of interpolation schemes for image deformation methods in PIV*. Experiments in fluids 2005, **38**, p. 233
28. Astarita T. *Analysis of interpolation schemes for image deformation methods in PIV: effect of noise on the accuracy and spatial resolution*. Experiments in fluids 2006, **40**, p. 977
29. Astarita T. *Analysis of weighting windows for image deformation methods in PIV*. Experiments in fluids 2007, **43**, p. 857
30. Mi J. et al. *PIV measurements of a turbulent jet issuing from round sharp-edged plate*. Experiments in fluids 2007, **42**, p. 625